JACS
JOURNAL OF THE AMERICAN CHEMICAL SOCIETY
Article
pubs.acs.org/JACS

Ultrafast Two-Electron Transfer in a CdS Quantum Dot–Extended-Viologen Cyclophane Complex

Ryan M. Young,*[,†,‡] Stephen C. Jensen,[†,‡] Kedy Edme,[†,‡] Yilei Wu,[†,‡] Matthew D. Krzyaniak,[†,‡] Nicolaas A. Vermeulen,[†] Edward J. Dale,[†] J. Fraser Stoddart,[†] Emily A. Weiss,[†,‡] Michael R. Wasielewski,*[,†,‡] and Dick T. Co*[,†,‡]

[†]Department of Chemistry and [‡]Argonne-Northwestern Solar Energy Research (ANSER) Center, Northwestern University, Evanston, Illinois 60208-3113, United States

Supporting Information

ABSTRACT: Time-resolved optical spectroscopies reveal multielectron transfer from the biexcitonic state of a CdS quantum dot to an adsorbed tetracationic compound cyclobis-(4,4′-(1,4-phenylene) bipyridin-1-ium-1,4-phenylene-bis-(methylene)) (**ExBox**$^{4+}$) to form both the **ExBox**$^{3+\bullet}$ and the doubly reduced **ExBox**$^{2(+\bullet)}$ states from a single laser pulse. Electron transfer in the single-exciton regime occurs in 1 ps. At higher excitation powers the second electron transfer takes ∼5 ps, which leads to a mixture of redox states of the acceptor ligand. The doubly reduced **ExBox**$^{2(+\bullet)}$ state has a lifetime of ∼10 ns, while CdS$^{+\bullet}$:**ExBox**$^{3+\bullet}$ recombines with multiple time constants, the longest of which is ∼300 μs. The long-lived charge separation and ability to accumulate multiple charges on **ExBox**$^{4+}$ demonstrate the potential of the CdS:**ExBox**$^{4+}$ complex to serve as a platform for two-electron photocatalysis.

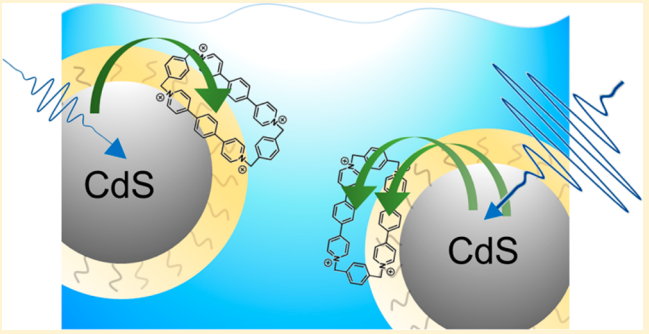

INTRODUCTION

Semiconducting quantum dots (QDs) offer a promising avenue for efficient solar energy conversion because of their size-tunable electronic and optical properties. QDs have high extinction coefficients for the formation of their lowest-energy excitons,[1] band gaps that span the visible and near-infrared (NIR) regions, and long excited-state lifetimes (tens of ns to μs).[2] All of these properties make QDs well-suited for photocatalyic and photovoltaic applications, which require both efficient light harvesting and delivery of charge to a suitable acceptor, often in the form of an adsorbed molecule.[3−10] For these applications, it is critical to have donor–acceptor pairs that produce long-lived charge-separated states upon photoexcitation. Additionally, for conversion of solar energy to liquid fuel, multiple electrons must be transferred to and stored at a given site in order to perform the desired chemical transformations that generally occur on the nanosecond time scale.[11] Ideally, photoexcitation of the QD would result in multiple essentially simultaneous charge transfers such that either the QD or a molecular redox shuttle accumulates multiple redox equivalents. While several studies have described the dissociation of multiexciton states within QDs to yield one-electron reductions of multiple adsorbed electron acceptors per QD,[4,5,8,12−15] in this paper we present direct observation of two-electron transfer (ET) from a QD to a single acceptor ligand from the biexciton state of a CdS QD generated by a high-power laser pulse.

Viologens, and in particular methyl viologen (**MV**$^{2+}$), are frequently studied in QD complexes because of their strong surface binding, relatively mild reduction potentials (−0.36 V vs Ag/AgCl for **MV**$^{2+}$), and the clear visible spectral signatures of the monoreduced states.[5−7,14,16,17] However, the more negative second reduction potential of **MV**$^{2+}$ (−0.76 V vs Ag/AgCl), and the lack of a low-energy absorption of the neutral **MV**^{0}, makes two-ET in **MV**$^{2+}$-containing systems more challenging.[18] The extended viologen cyclophane, cyclobis(4,4′-(1,4-phenylene)bipyridin-1-ium-1,4-phenylenebis (methylene)) tetrachloride[19] (**ExBox**·4Cl in Figure 1), avoids these issues and possesses many desirable properties for application in QD-based systems.[20,21] Specifically, **ExBox**$^{4+}$ has four relatively mild reduction potentials (two sets of two one-electron reductions, the first of which occurs at −0.59 V and the second at −0.72 V vs Ag/AgCl in DMF)[19] that allow it to accept up to four electrons. The phenyl spacing group in the extended viologen arms electronically decouples the pyridinum subunits, which reduces the splitting between the first two reduction potentials and makes the extended viologen a promising candidate for ultrafast multielectron transfer. Additionally, the various reduced states of **ExBox**$^{4+}$ exhibit strong visible and NIR absorption bands[22,23] and, as such, are easily identified in transient absorption experiments. Electron paramagnetic resonance (EPR) investigations on similar cyclophanes such

Received: December 22, 2015
Published: April 25, 2016

DOI: 10.1021/jacs.5b13386
J. Am. Chem. Soc. 2016, 138, 6163−6170

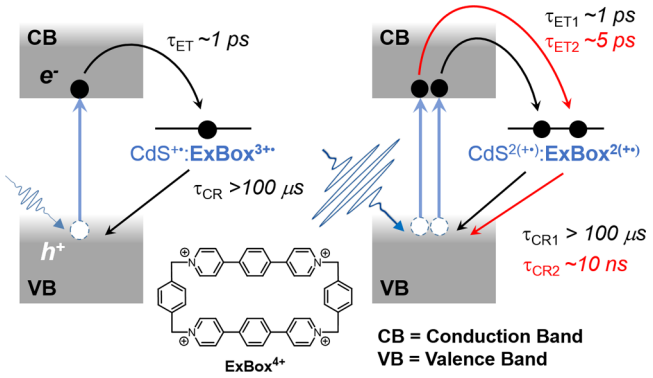

Figure 1. Schematic of photoinduced charge transfer in the electrostatically bound complex CdS:**ExBox**$^{4+}$.

as cyclobis(paraquat-*p*-phenylene) show[24] that, upon reduction, the unpaired electron hops between the two equivalent bipyridinium units faster than ~100 ns, a situation that can dramatically extend the lifetime of the charge-separated state. The cyclophane geometry also reduces the Coulombic repulsion associated with a multiply reduced state compared to a simple viologen, which in turn increases the thermodynamic driving force for photoinduced ET. In this paper, we utilize **ExBox**$^{4+}$ as a charge-accumulation ligand and demonstrate two-ET by monitoring the unique absorption band of the diradical **ExBox**$^{2(+\bullet)}$ using transient absorption spectroscopy. Figure 1 shows a schematic of the power-dependent charge-transfer processes.

We study the dynamics of ET in a 1:1 mixture of CdS QDs (4.1 μM, radius =1.8 nm) with **ExBox**·4Cl in water (pH 7), hereafter referred to as CdS:**ExBox**$^{4+}$. 3-Mercaptopropionic acid (3-MPA) serves as the solubilizing surface ligand for the QDs. Figure S2B shows the absorption spectra of the QDs and the CdS:**ExBox**$^{4+}$ samples: the peak at 406 nm corresponds to the first excitonic transition of the QDs, while, in the mixture, higher absorption in the ultraviolet region corresponds to **ExBox**$^{4+}$. Additionally, we study 1:1 mixtures of QDs with the benzylated extended viologen, 4,4′-(1,4-phenylene)bis(1-benzylpyridin-1-ium) dichloride (**BnExV**·2Cl), to test how the ability of the electron to hop between sites on the acceptor affects the ET dynamics compared to a single-sided acceptor with nearly identical reduction potentials.

EXPERIMENTAL DETAILS

Synthesis of ExBox·4Cl and BnExV·2Cl. We synthesized **ExBox**·4Cl according to literature procedures[19,25] and details of the synthesis of **BnExV**·2Cl are in the Supporting Information (SI).

Synthesis and Purification of CdS Quantum Dots. We first prepared the Cd:Oleate precursor by heating 0.256 g CdO (Sigma-Aldrich #244783), 13.7 mL octadecene (ODE, Sigma-Aldrich, 90%, #O806), and 6.3 mL oleic acid (OA, Sigma-Aldrich, 90%, #364525) in a three-neck round-bottom flask to 250 °C under a flow of nitrogen gas until all CdO (which is a deep red) was converted to Cd:Oleate (which is colorless). Upon cooling the Cd:Oleate solution to room temperature, we transferred 4 mL of the solution to 6 mL octadecene in a round-bottom flask. The solution was heated to 260 °C and injected 2 mL 0.10 M sulfur in ODE, and the temperature was reduced to 220 °C. The QDs nucleated for 45 s, and the size was verified by the wavelength of the first electronic absorption peak.[1] The cooled QD solution was purified by distributing the solution into 4 × 15 mL centrifuge tubes and then adding 3:1 (v:v) acetone:QDs. We centrifuged the samples for 3500 rpm for 5 min, then discarded the supernatant, resuspended the pellet of QDs in 1.5 mL hexanes, and then added 3:1 (v:v) methanol:QDs. After a second centrifugation at 3500 rpm for 5 min, we discarded the supernatant and redispersed the QDs in chloroform.

In order to suspend the CdS QDs in water, a ligand exchange is necessary to replace the oleate ligands with 3-mercaptopropionic acid. We concentrated a quarter of a batch of QDs so that the total volume is <0.2 mL. We then added 0.125 mL 3-mercaptopropionic acid (Sigma-Aldrich >99%, #M5801), 1.5 mL methanol, and 1.75 mL Triton B (Sigma-Aldrich, 40 wt % in methanol, #B32602). Triton B facilitates thiol deprotonation, which enables the ligand exchange to occur. We stirred the sample for 2 h and then added it to a 15 mL centrifuge tube with 5 mL ethyl-ether (Sigma-Aldrich, 99%, #422177) and 5 mL ethyl acetate (Sigma-Aldrich, 99.8%, #270989). The solution was centrifuged at 3500 rpm for 5 min, then the supernatant was discarded, and the QDs resuspended in 4 mL methanol. We added 5 mL ethyl ether and 5 mL ethyl acetate, shook the vials, and centrifuged them again at 3500 rpm for 5 min. Finally, we discarded the supernatant and resuspended the QDs in methanol.

Preparation of CdS:ExBox^{4+} and CdS:BnExV^{2+} Complexes. We determined the concentration of CdS by comparing the first absorption peak against published sizing curves.[1] Once the concentration of the QDs was determined in methanol, the appropriate amount was added to a 3 mL glass vial, and the solution was dried under a stream of N_2 gas and resuspended in Milli-Q Water (18.2 MΩ·cm). Either **ExBox**·4Cl or **BnExV**·2Cl was added to the sample from a 1.06 mM stock solution (in water), depending on the desired complex, the sample was then degassed with nitrogen, and the solution was transferred to a 0.2 cm quartz cuvette in a nitrogen box and allowed to equilibrate for 12 h prior to optical experiments. The adsorption of **ExBox**$^{4+}$ and **BnExV**$^{2+}$ on the CdS QD's surface is limited by the binding affinity of the ligands for the QD, such that in a 1:1 solution we expect a distribution of populations with the majority of complexes being 1:1 CdS:**ExBox**$^{4+}$ (or CdS:**BnExV**$^{2+}$), some QDs with more than one **ExBox**$^{4+}$ (or **BnExV**$^{2+}$) bound to the surface, and some QDs with no bound acceptor. As such, the transient experiments sample the mixture of complexes present in solution.

METHODS

The SI contains details on our experimental apparatuses and methods.

RESULTS AND DISCUSSION

One-Electron Transfer Dynamics. First, we explore the thermodynamically accessible one-ET pathway from the CdS QD to **ExBox**$^{4+}$ in the single-exciton regime ($\Delta G_{ET} \sim -0.1$ eV, see SI). Figure 2A shows the femtosecond transient absorption (fsTA) spectra of CdS:**ExBox**$^{4+}$ upon selectively exciting the QDs at 414 nm ($1S_h-1S_e$ exciton transition) with an excitation density of $\langle N \rangle = 0.02$ excitons per QD (see SI for details). At this fluence, only the single ET process is accessible. Immediately after excitation, strong absorption bands at 488, 522, 980, and 1140 nm appear corresponding to the photoinduced absorptions of the reduced **ExBox**$^{3+\bullet}$.[22] At early times, there is a weak unstructured transient signal similar to that observed for 3-MPA-coated CdS QDs (see Figure S7) that decays quickly in the NIR region, but in the visible spectrum is effectively constant for the duration of the fsTA experiment. The apparent fast decays of the **ExBox**$^{3+\bullet}$ signal in the NIR region are likely a consequence of hole relaxation[26] following ET from the QD to the acceptor. Additionally, parallel excitation and subsequent hole relaxation of a small population of CdS QDs with no adsorbed quenchers may contribute to the apparent decay.

To examine the ET dynamics, we monitor the amplitude of the **ExBox**$^{3+\bullet}$ $D_n \leftarrow D_1$ transition;[22] these bands continue to rise after excitation, reach a maximum near 50 ps, and persist throughout the 8 ns time window of the fsTA experiment.

DOI: 10.1021/jacs.5b13386
J. Am. Chem. Soc. 2016, 138, 6163−6170

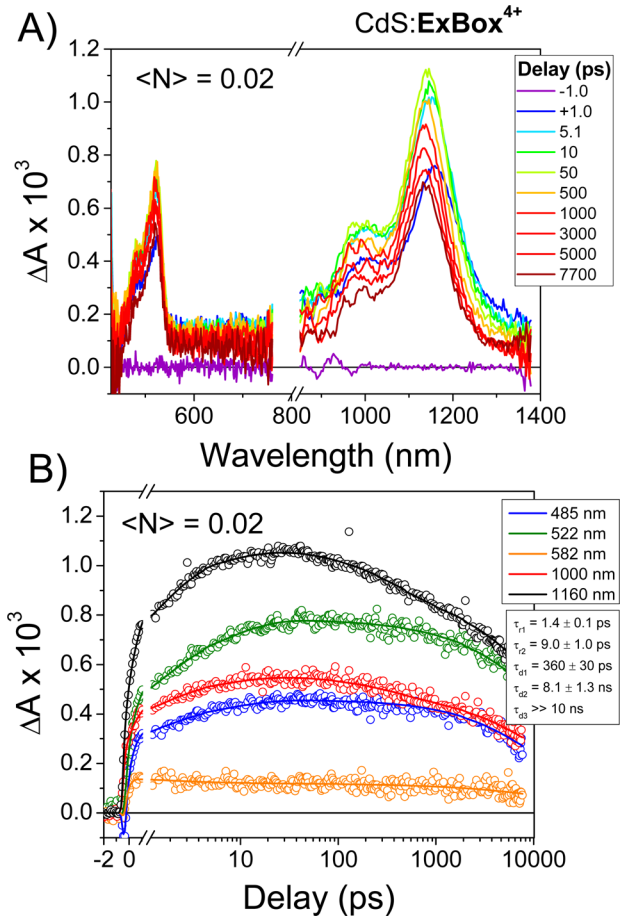

Figure 2. (A) fsTA spectra of CdS:**ExBox**$^{4+}$ following 414 nm excitation at $\langle N \rangle = 0.02$ (50 μW). Data near the 830 nm fundamental scatter are suppressed for clarity. (B) Kinetic fits of selected wavelengths to a multiexponential decay convoluted with a Gaussian instrument response. Lifetimes of rising and decaying components are denoted τ_{rx} and τ_{dx}, respectively.

Global fits of selected wavelengths presented in Figure 2B show that ET from the excited CdS QD to the ligand occurs with two time constants, ~1.4 ± 0.1 and 9 ± 1 ps, and the charges recombine with several components, the fastest of which is 360 ± 30 ps. The observation of ultrafast ET to **ExBox**$^{4+}$ strongly suggests that the extended viologen subunit is in direct contact with the CdS surface, permeating the short 3-MPA shell and facilitating strong electronic coupling between the **ExBox**$^{4+}$ LUMO and the exciton wave function.[27] The two discernible ET time constants extracted from the global fit probably correspond to two sets of adsorption geometries of the CdS:**ExBox**$^{4+}$ complex with different magnitudes of electronic coupling. Low-fluence excitation of 3-MPA CdS QDs (Figures S7 and S9) reveals that the fastest competing exciton decay process (k_X) is $k_X \sim (17\ \text{ns})^{-1}$, which implies that the quantum yield of ET for small $\langle N \rangle$ is near unity:

$$\Phi_1 = \left(\frac{k_1}{k_1 + k_X}\right) \approx 1 \qquad (1)$$

The slower of the two observed rises (9 ps) also leads to near unity quantum yield.

Femtosecond stimulated Raman spectroscopy (FSRS) on these samples corroborates the ET dynamics. Following actinic excitation at 400 nm (1S exciton transition) and using a Raman pump at 530 nm (resonant with the **ExBox**$^{3+\bullet}$ $D_n \leftarrow D_1$ transition), we observe the rapid growth of Raman lines associated with **ExBox**$^{3+\bullet}$.[22] These bands again exhibit biexponential growth without any apparent spectral shifts (see Figure S24). Global fits to these bands reveal ET rates of 1.2 ± 0.2 and 8.8 ± 1.5 ps, in excellent agreement with the fsTA data. This behavior suggests that the ligand does not undergo significant geometric change upon reduction and supports the assignment that the biexponential rise observed in the fsTA experiment owes to multiple populations transferring charge.

As the fsTA data show, the initial charge recombination (CR) occurs on the ns time scale. We use nanosecond transient absorption (nsTA) spectroscopy (Figure S19) to further investigate CR of the CdS$^{+\bullet}$:**ExBox**$^{3+\bullet}$ ion pair. Multiexponential fits presented in Figure 3A show that CR occurs

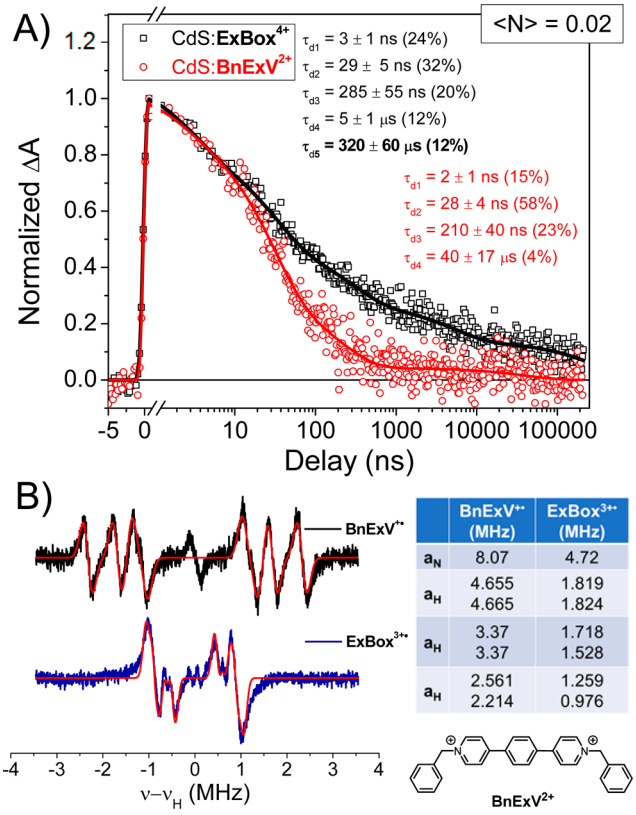

	BnExV$^{+\bullet}$ (MHz)	ExBox$^{3+\bullet}$ (MHz)
a_N	8.07	4.72
a_H	4.655 4.665	1.819 1.824
a_H	3.37 3.37	1.718 1.528
a_H	2.561 2.214	1.259 0.976

Figure 3. (A) Normalized kinetic traces for CdS$^{+\bullet}$:**ExBox**$^{3+\bullet}$ (black, λ_{probe} = 522 nm) and CdS$^{+\bullet}$:**BnExV**$^{+\bullet}$ (red, λ_{probe} = 518 nm) with $\langle N \rangle$ = 0.02, with multiexponential fits shown in solid lines. (B) cw-ENDOR spectra of chemically reduced **BnExV**$^{+\bullet}$ and **ExBox**$^{3+\bullet}$ in DMF. The simulated spectra (red lines) show that the ENDOR lines are split due to inhomogeneity in the proton environments. The hyperfine couplings of **ExBox**$^{3+\bullet}$ are approximately one-half those of **BnExV**$^{+\bullet}$, which indicates that the spin density is distributed across the cyclophane on the ENDOR time scale.

with multiple time constants that span from ~3 ns to hundreds of μs. From the nsTA data, we see that 24% of the CdS$^{+\bullet}$:**ExBox**$^{3+\bullet}$ population recombines with a 3 ± 1 ns time constant, 32% decays with a 29 ± 5 ns time constant and 20% decays with a 285 ± 55 ns time constant. The remaining population persists for many microseconds, with the longest extracted CR time for CdS$^{+\bullet}$:**ExBox**$^{3+\bullet}$ being 320 ± 60 μs (12%), which is exceptionally long. The lack of a comparable

DOI: 10.1021/jacs.5b13386
J. Am. Chem. Soc. 2016, 138, 6163−6170

hundreds of μs component in the CR lifetimes of the CdS$^{+\bullet}$:**BnExV**$^{+\bullet}$ ion pair suggests that the long ~320 μs lifetime in the CdS:**ExBox**$^{4+}$ sample is related to the rigid geometry of the **ExBox**$^{4+}$ cyclophane. We observe for CdS$^{+\bullet}$:**BnExV**$^{+\bullet}$ that the majority of the CR occurs within the first tens of nanoseconds (15% in 2 ± 1 ns and 58% in 28 ± 4 ns) and 23% occurs within 210 ± 40 ns. There is a minor (4%) component that recombines with 40 ± 17 μs, however the low signal-to-noise ratio at these longest times limits interpretation of this feature. No evidence for recombination to the triplet state of **ExBox**$^{4+}$ is observed in either the fs- or nsTA experiments.[23]

Electron-nuclear double resonance (ENDOR) spectroscopy of chemically generated, singly reduced **ExBox**$^{3+\bullet}$ and **BnExV**$^{+\bullet}$ offers further insight into the nature of the long lifetime of CdS$^{+\bullet}$:**ExBox**$^{3+\bullet}$ and the effect of the cofacially dimeric nature of the cyclophane versus the monomeric extended viologen on the CR lifetimes. The ENDOR spectra for **ExBox**$^{3+\bullet}$ and **BnExV**$^{+\bullet}$ shown in Figure 3B each exhibit three principle sets of lines, one for each equivalent proton. The lines for **ExBox**$^{3+\bullet}$ appear at lower frequency shifts than those of **BnExV**$^{+\bullet}$, which indicates smaller hyperfine couplings in the cyclophane. If the spin density of a radical electron is evenly shared across two sites on the ~70 ns time scale of the ENDOR measurement, then the hyperfine couplings—the interactions of the radical electron spin with the adjacent nuclear spins—will be reduced by half.[28,29] Figure 3B shows that these hyperfine couplings are indeed approximately a factor of 2 smaller for **ExBox**$^{3+\bullet}$ than for **BnExV**$^{+\bullet}$. The electron hopping rate is estimated to be $k_{hop} \geq (70\ ns)^{-1}$ based on the ~14 MHz ENDOR frequency, and as such any fraction of CdS$^{+\bullet}$:**ExBox**$^{3+\bullet}$ that survives recombination for several hundred nanoseconds will experience a competitive process to charge recombination. CR for this population is thus slowed by the hopping of the electron between the two equivalent viologen arms on either side of the cyclophane,[24] which delays the CR process by reducing the average electronic coupling.

Two-Electron Transfer Dynamics. With the dynamics in the single-exciton regime established, we next focus on the pump-fluence dependence of ET. Figure 4 shows the fsTA spectrum of CdS:**ExBox**$^{4+}$ at 50 ps (at which point the single ET process is complete) for different excitation powers overlaid with steady-state spectra of **ExBox**$^{3+\bullet}$ (dark gray) and **ExBox**$^{2(+\bullet)}$ (light gray) obtained after chemical reduction with cobaltacene ($CoCp_2$). Higher reductions are not considered because the number of photoinduced reduction events is ultimately limited by the 2-fold degeneracy of the conduction band for CdS QDs at this pump wavelength.[30] As the excitation density increases, the intensities of the 488 and 980 nm bands (marked with arrows) also increase relative to the 522 and 1140 nm bands, respectively, and the overall line shape approaches that of the steady-state spectrum of **ExBox**$^{2(+\bullet)}$. Most strikingly, a new, distinct band at 588 nm emerges at high fluence that we also observe in the **ExBox**$^{2(+\bullet)}$ steady-state spectrum. The absorption spectra show that the extinction coefficient of **ExBox**$^{2(+\bullet)}$ at 522 nm is ~69,000 L cm^{-1} M^{-1}, approximately twice as large as that of **ExBox**$^{3+\bullet}$ (32,000 L cm^{-1} M^{-1}, Figure S4). The situation is similar for the NIR bands and indicates that the first- and second-ET dynamics cannot be easily distinguished at these wavelengths.

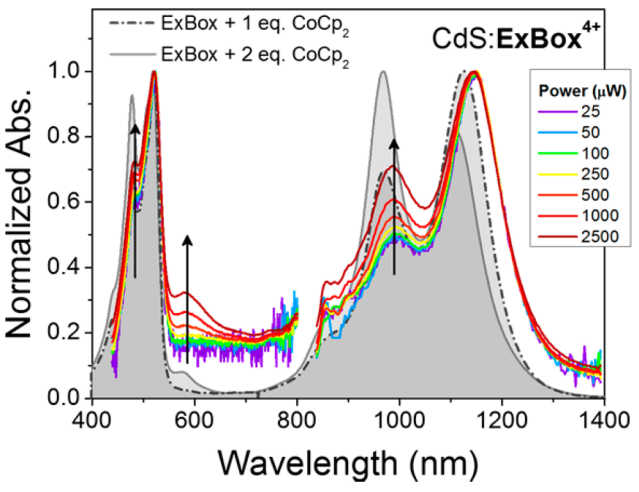

Figure 4. Overlay of normalized fsTA spectra of CdS:**ExBox**$^{4+}$ at +50 ps for different excitation powers (color lines) and the steady-state absorption spectra of chemically reduced **ExBox**$^{3+\bullet}$ (dark-gray, dash-dot) and **ExBox**$^{2(+\bullet)}$ (light-gray solid line).

Figure 5A shows the fsTA spectra acquired with high excitation fluence (1.0 mW, $\langle N \rangle$ = 0.37). At this higher excitation density, ~ 10% of the QD excited-state population is capable of transferring two electrons (*vide infra*). The 588 nm transition, characteristic of the doubly reduced **ExBox**$^{2(+\bullet)}$, appears within the first few ps in the fsTA data and decays throughout the 8 ns experimental window. The early appearance of the transient feature at 588 nm indicates that the second charge transfer must also be rapid, as it at least partially outcompetes higher-order deactivation processes available to the biexciton and trion states (*vide infra*). Importantly, the fsTA spectra do not at any time demonstrate the full peak inversion between the NIR bands of the singly and doubly reduced states seen in the steady-state spectra, which indicates a mixture of redox states is present throughout the entire time range.

The dynamics of **ExBox**$^{2(+\bullet)}$ formation can be disentangled by focusing on the unique 588 nm band. To separate this signal from the background of QD and CdS$^{+\bullet}$:**ExBox**$^{3+\bullet}$ populations, we take the integrated ΔA intensity following spline subtraction of the fsTA spectra between two fixed wavelengths at each pump−probe delay (black circles in Figure 5A, see SI for details) and compare the time evolution to the one-ET dynamics established at low excitation power (*vide supra*). Figure 5B gives the results of this analysis for $\langle N \rangle$ = 0.37. This 588 nm signal rises more slowly and reaches a maximum at an earlier time compared to the corresponding one-ET population, which is indicative of slower ET and faster recombination for the second electron. Exponential fits show that the 588 nm band rises with an effective rate constant of k_{eff} = (4.6 ± 0.2 ps)$^{-1}$, compared to (~1 ps)$^{-1}$ for single ET.

In principle, the doubly reduced state can form either by direct, concerted two-ET or by sequential transfer following biexciton dissociation. We use k_1 = (1 ps)$^{-1}$ for the biexciton dissociation rate, as previous studies have shown that the rate of single ET is effectively independent of exciton order.[14] If the **ExBox**$^{2(+\bullet)}$ state is formed directly from the biexciton state, then the effective rate of its appearance must necessarily be faster than the biexciton dissociation rate, as the rate constants are additive. Since, instead, we see the **ExBox**$^{2(+\bullet)}$ band rise much more slowly, we conclude that the rate of simultaneous ET is in fact quite small compared to (1 ps)$^{-1}$ and that the **ExBox**$^{2(+\bullet)}$ forms sequentially following biexciton dissociation.

DOI: 10.1021/jacs.5b13386
J. Am. Chem. Soc. 2016, 138, 6163−6170

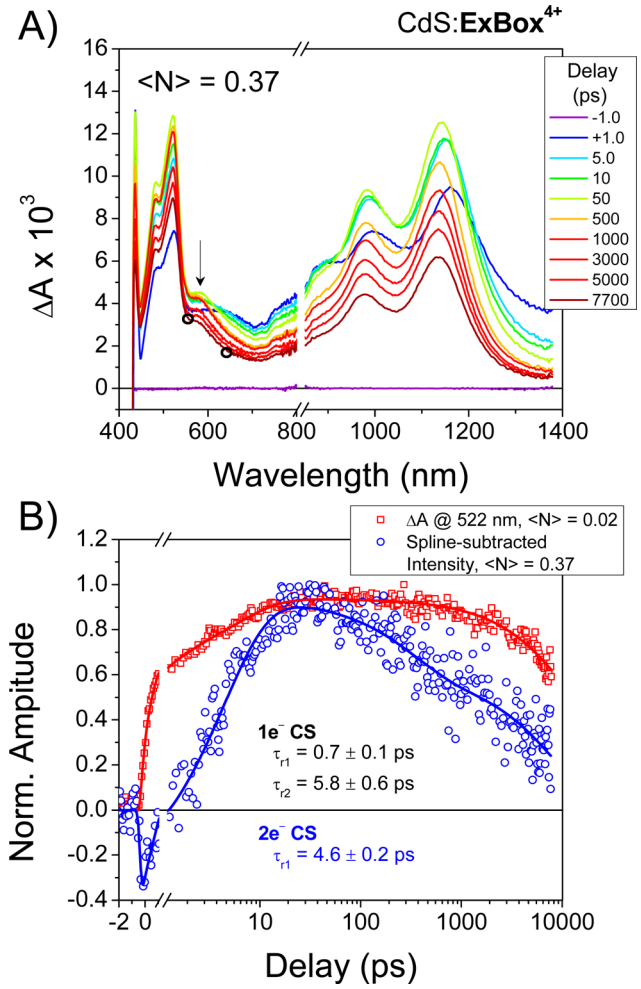

Figure 5. (A) fsTA spectra of CdS:**ExBox**$^{4+}$ for $\langle N\rangle$ = 0.37 (1.0 mW). At this higher excitation density, a new band emerges at 588 nm (marked with an arrow) characteristic of **ExBox**$^{2(+\bullet)}$. Black circles indicate the wavelengths for spline-subtraction. (B) Comparison of the normalized spline-subtracted signal for CdS$^{2(+\bullet)}$:**ExBox**$^{2(+\bullet)}$ at $\langle N\rangle$ = 0.37 (blue) with the ΔA for CdS$^{+\bullet}$:**ExBox**$^{3+\bullet}$ obtained at $\langle N\rangle$ = 0.02 (red), which shows that the second ET is slower than the first ET process by a factor of ∼5. See the SI for recombination times.

The rate of formation is thus controlled by the competitive rates experienced by the trion following dissociation: second ET (k_2) and trion decay (k_{X+}). Therefore, $k_{\text{eff}} = k_2 + k_{X+}$. We estimate $k_{X+} = (130 \pm 30\ \text{ps})^{-1}$ (*vide infra*), which yields a value of $k_2 = (4.8 \pm 0.2\ \text{ps})^{-1}$. We note that the second ET rate is slower than the single ET rate in CdS:**BnExV**$^{2+}$ $(2.2 \pm 0.5\ \text{ps})^{-1}$ (Figure S12). Sequential ET to the second arm of **ExBox** is expected to proceed with half the rate of the first transfer, since there are statistically half as many equivalent acceptors. The disparity between this rate and the effective rise of the 588 nm band may suggest that presence of the first charge slightly alters the reduction potential and slows the rate of ET. The slower second ET in CdS:**ExBox** is consistent with previously reported multielectron transfer rates for a similar but smaller viologen cyclophane adsorbed to TiO_2 nanoparticles; in that case, however, the rates could not be fully separated due to overlapping absorptions.[31,32]

Decay of the 588 nm band by CR occurs with two components: 300 ps (∼40%) and >8 ns (∼60%). Accurate recombination times for the second electron could not be obtained, as the **ExBox**$^{2(+\bullet)}$ absorption at 588 nm is not clearly observable in the nsTA spectra, but we estimate the longer recombination time to be at least ∼10 ns (Table S2). The lack of an obvious isosbestic point between the **ExBox**$^{3+\bullet}$ and **ExBox**$^{2(+\bullet)}$ bands in the fsTA data may suggest that the two electrons in the doubly reduced species recombine in parallel. Similar experiments on CdS:**BnExV**$^{2+}$ were limited due to sample instability at high excitation fluence, so it remains unclear if the cyclophane is extending the two-electron CR time as well.

While the quantum yield of ET in the single exciton regime is near unity, the situation is more complex at higher $\langle N\rangle$ because of the multitude of competing decay pathways for the population of biexcitons in the highly excited QD. We calculate the quantum yields for the first and (sequential) second ET events at higher $\langle N\rangle$ using the kinetics discussed above and show the relevant processes in Figure 6A. At high excitation

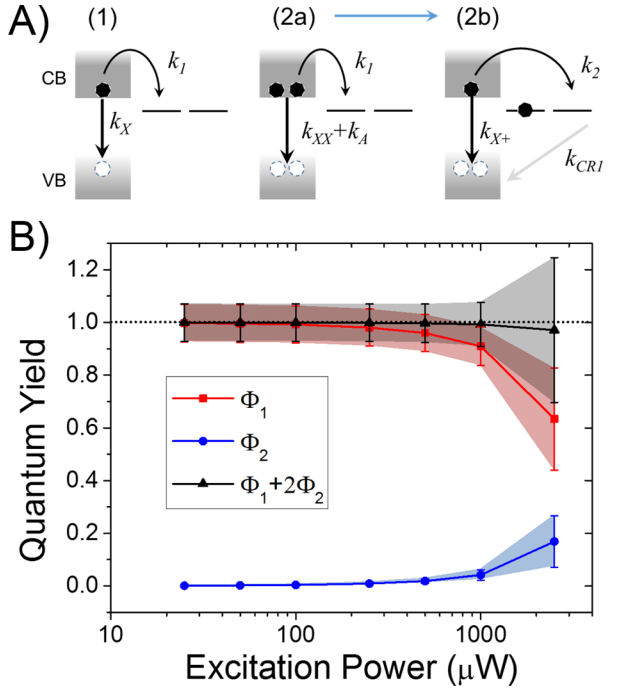

Figure 6. (A) ET in the single exciton regime (1) where rate k_1 vastly outcompetes exciton decay with rate k_X. Sequential two-ET proceeds from the initial biexciton state (2a) to the intermediate CdS$^{+\bullet}$:**ExBox**$^{3+\bullet}$ state (2b) with rate k_1. The biexciton also decays via k_{XX} and k_A. From (2b), the trion dissociates to CdS$^{2(+\bullet)}$:**ExBox**$^{2(+\bullet)}$ with rate k_2 or decays via k_{X+}. CR k_{CR1} is neglected as it is several orders of magnitude smaller than k_2. Intermediate (hot) single exciton state produced by Auger decay not shown. (B) Quantum yields for the first and second ET as a function of excitation power.

density, the quantum yields per photon of the first (Φ_1) and second (Φ_2) ET from the QD to **ExBox** are

$$\Phi_1 = a_1\left(\frac{k_1}{k_1 + k_X}\right) + \frac{a_2}{2}\left[\left(\frac{k_A}{k_1 + k_{XX} + k_A}\right)\left(\frac{k_1}{k_1 + k_X}\right) + \left(\frac{k_1}{k_1 + k_{XX} + k_A}\right)\left(\frac{k_{X+}}{k_2 + k_{X+}}\right)\right] \quad (2)$$

and

DOI: 10.1021/jacs.5b13386
J. Am. Chem. Soc. 2016, 138, 6163−6170

$$\Phi_2 = \frac{a_2}{2}\left(\frac{k_1}{k_1 + k_{XX} + k_A}\right)\left(\frac{k_2}{k_2 + k_{X+}}\right) \quad (3)$$

where k_1 and k_2 are the first and second ET rates, respectively, and k_X, k_{XX}, k_A, and k_{X+} are the single exciton, biexciton, Auger, and trion decay rates, respectively. The coefficients a_1 and a_2 describe the fraction of excited QDs initially in the single and biexciton states, respectively. The initially prepared excited state of the QD is a mixture of single excitons ($j = 1$) and biexcitons ($j = 2$), as prescribed by the binomial distribution, P_j, such that the fraction of initial population in each state is $a_1 = P_1/(P_1 + P_2)$ and $a_2 = P_2/(P_1 + P_2)$, respectively. The binomial distribution accurately models the behavior of the QDs near excitation saturation and permits a maximal exciton population of 2, as required by the 2-fold degeneracy of the CdS conduction band. The contribution to the quantum yield from a_2 is divided in half since the creation of each biexciton state requires two photons. Eq 2 is a generalization of eq 1 to include contributions to **ExBox**$^{3+\bullet}$ from both the single and biexciton states: at low $\langle N\rangle$ $a_1 \approx 1$ and $a_2 \approx 0$. There are two indirect, additive contributions to Φ_1 from the biexciton state: single ET following Auger decay of the biexciton and trion decay following the first ET. For the contribution arising from Auger decay, we take the yield of single excitons produced by Auger decay multiplied by the yield of single ET to the acceptor, assuming that the single ET rate and the (hot) exciton decay rate here are the same as those in the low $\langle N\rangle$ case. We add the contribution from the trion state by taking the joint probability of creating the trion (state 2b in Figure 6A) and of the trion decaying to the ground state, leaving a total of one electron in the acceptor. The biexciton decay rate k_{XX} is typically on the order of 10 ps,[33−35] much more rapid than the single exciton decay rate. From fsTA data of CdS QDs with no acceptor at $\langle N\rangle = 0.08$, we estimate an upper bound for the biexciton decay as $k_{XX} = (32 \pm 7\ \text{ps})^{-1}$, which is similar to values reported for biexciton decay in comparably sized CdSe QDs.[36,37] For sequential two-ET, the first ET step leaves the QD in a positive trion state, which decays more slowly with a rate approximated[37−39] as $k_{X+} \sim k_{XX}/4 = (130 \pm 30\ \text{ps})^{-1}$ (see Figure S9). We approximate k_A by using the decay of the CdS QD signal at $\langle N\rangle = 0.37$ and considering that at this power the observed rate contains contributions from k_{XX} and k_A. With the value for k_{XX} discussed above, the observed $(16\ \text{ps})^{-1}$ decay rate for $\langle N\rangle = 0.37$ yields an estimate of $k_A = (32 \pm 9\ \text{ps})^{-1}$ (see SI). We neglect CR, as Figures 2 and 5 indicate that the fastest component of CR is 2 orders of magnitude slower than either ET process. Comparison of the kinetic fits for the complex at low and high powers (Figure S11) demonstrates that the fast rate of ET is near $(1\ \text{ps})^{-1}$ in both cases and that the initial (first) ET rate is not strongly dependent on $\langle N\rangle$.

Figure 6B shows the results at using $k_1 = (1.4\ \text{ps})^{-1}$ and $k_2 = (4.8\ \text{ps})^{-1}$ as a function of excitation power. At low excitation powers, Φ_1 is 0.99, in keeping with the single ET discussion. However, Φ_1 in eq 2 now explicitly accounts for the fraction of excited population in the single-exciton state (a_1), which at the lowest excitation power (25 μW) is 0.99. As the excitation power increases, the relative number of biexcitons increases, leading to a further decrease in Φ_1 and a concomitant rise in Φ_2. Importantly, the total quantum yield of ET events, $\Phi_1 + 2\Phi_2$, slightly decreases with increasing excitation power, since the higher fraction of population in the biexciton state is exposed to faster decay pathways k_A, k_{XX}, and subsequently k_{X+}, and creating a higher population of biexcitons requires the absorption of more photons. At the highest power measured, the total efficiency of ET reduces to 0.97, and roughly one-third of the excited electrons ($2\Phi_2 = 34\%$) become associated with **ExBox**$^{2(+\bullet)}$. The fraction of population in the biexciton state immediately after excitation (a_2) is 38%, which demonstrates the impact of the faster nonradiative decay pathways accessible to the biexciton on the ET process. Despite this, the individual quantum yields are still quite high despite the modest ΔG_{ET} for both ETs.

We can compute the absolute concentration of (singly and doubly) reduced species c present at time t, since the population of each reduced state is produced according to the respective kinetics described above. For a 1:1 complex, after all ET processes are complete, the total concentration of reduced **ExBox** ligands following excitation is

$$c = \frac{\Delta A(t)}{l[\varepsilon_1 \Phi'_1 f_1(t) + \varepsilon_2 \Phi'_2 f_2(t)]} \quad (4)$$

where l is the optical path length (2 mm), and $f_j(t)$ describes the normalized populations as a function of time t to account for any recombination at the time of analysis (see SI for details). Φ'_j is the product yield for ET to **ExBox**$^{3+\bullet}$ ($j = 1$) and to **ExBox**$^{2(+\bullet)}$ ($j = 2$), respectively, per exciton or biexciton (not per photon). The product yields Φ'_j differ from the quantum yields by not including the factor of 1/2 in front of a_2 that normalizes the yield per absorbed photon. Using c, we determine the individual concentrations of **ExBox**$^{3+\bullet}$ and **ExBox**$^{2(+\bullet)}$, c_1 and c_2, respectively, and thus the number of reductive equivalents delivered to **ExBox**$^{4+}$ per QD as

$$n_{red} = \frac{c_1 + 2c_2}{c_{QD}} = \frac{\Phi'_1 c + 2\Phi'_2 c}{c_{QD}} \quad (5)$$

where c_{QD} is the QD concentration (4.1 μM). Figure 7 shows values of n_{red} obtained at two different probe wavelengths as a function of excitation power at 50 ps, near the maxima of both populations. We see that the values saturate at high laser powers and approach $n_{red} = 1$. The fact that the curve does not saturate at $n_{red} = 2$ is consistent with the observation that not all QDs in solution are complexed with **ExBox**$^{4+}$, effectively reducing the number of QDs participating in the photochemistry and inflating c_{QD} in eq 5. Overall, the reductive

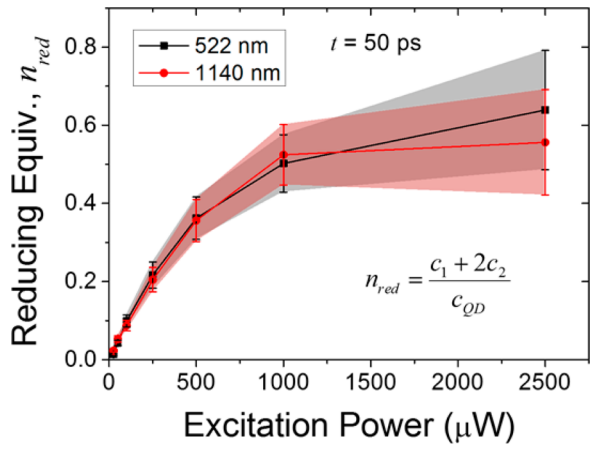

Figure 7. Number of reducing equivalents per QD (n_{red}) as a function of excitation power for two different probe wavelengths at $t = 50$ ps, long after all ET processes are complete.

DOI: 10.1021/jacs.5b13386
J. Am. Chem. Soc. 2016, 138, 6163−6170

efficiency of **ExBox** is reasonably high in this system, which, when combined with the long lifetime of both its singly and doubly reduced states, make it well-suited as a model redox shuttle.

CONCLUSION

We have demonstrated the ability to reduce a single $\mathbf{ExBox}^{4+}$ ligand multiple times in a CdS:$\mathbf{ExBox}^{4+}$ complex with a single high-power laser pulse. The similarity of the first two reduction potentials in $\mathbf{ExBox}^{4+}$ gives the multiple ET events nearly identical driving forces and allows $\mathbf{ExBox}^{4+}$ to act as an electron "sink" with respect to the photoexcited QD. ET to $\mathbf{ExBox}^{4+}$ is ultrafast, which indicates that the cyclophane binds in close proximity to the QD surface, which further leads to near unit efficiency for ET in the single-exciton regime. Recombination is generally long, with the longest component fitting to a lifetime of 320 μs. The dimeric nature of the cyclophane also facilitates the long lifetime of $CdS^{+\bullet}$:$\mathbf{ExBox}^{3+\bullet}$ by sharing the electron between viologen units on time scales longer than ~70 ns. This finding gives insight into the design of highly efficient and very long-lived constructs for photoinduced charge separation. Multielectron transfer also occurs rapidly, in about 5 ps, and the doubly reduced state has a recombination time of ~10 ns, which provides a reasonable amount of time to serve as an effective two-electron redox shuttle. The quantum yields of ET depend on the excitation power and are both reasonably high. The quantum yield for doubly reduced $\mathbf{ExBox}^{2(+\bullet)}$ approaches 17% at the highest excitation fluence measured, where ~38% of the excited population is capable of transferring two electrons. With the electron accumulation properties of $\mathbf{ExBox}^{4+}$ and the fast ET rates within the CdS:$\mathbf{ExBox}^{4+}$ complex established, future work will focus on coupling $\mathbf{ExBox}^{4+}$ with a QD capable of multiple exciton generation as a means to transfer and store multiple charges with a single photon.[40] QDs with higher conduction band degeneracies may also provide access to higher redox states of $\mathbf{ExBox}^{4+}$ upon multiphoton excitation and can aid the rational design of multielectron redox shuttles.

ASSOCIATED CONTENT

Supporting Information

The Supporting Information is available free of charge on the ACS Publications website at DOI: 10.1021/jacs.5b13386.

Analysis and experimental details, including synthesis, electrochemistry, EPR, fsTA, nsTA, and FSRS (PDF)

AUTHOR INFORMATION

Corresponding Authors

*ryan.young@northwestern.edu
*m-wasielewski@northwestern.edu
*co@northwestern.edu

Notes

The authors declare no competing financial interest.

ACKNOWLEDGMENTS

Spectroscopic studies (R.M.Y., D.T.C., S.C.J., K.E., E.A.W., and M.R.W.) were supported as part of the ANSER Center, an Energy Frontier Research Center funded by the U.S. Department of Energy, Office of Science, Basic Energy Sciences, under Award no. DE-SC0001059. N.A.V., E.J.D., and J.F.S. are part of the Joint Center of Excellence in Integrated Nano-Systems at the King Abdulaziz City for Science and Technology and Northwestern University (NU). R.M.Y. and D.T.C. thank the Camille and Henry Dreyfus Postdoctoral Program in Environmental Chemistry for support. E.J.D. and K.E. are supported by a Graduate Research Fellowship (GRF) from the National Science Foundation. E.J.D. and Y.W. gratefully acknowledge support from the Ryan Fellowship and the NU International Institute for Nanotechnology. Y.W. thanks the Fulbright Scholars Program for a Graduate Research Fellowship.

REFERENCES

(1) Yu, W. W.; Qu, L.; Guo, W.; Peng, X. *Chem. Mater.* **2003**, *15*, 2854.
(2) de Mello Donegá, C.; Bode, M.; Meijerink, A. *Phys. Rev. B: Condens. Matter Mater. Phys.* **2006**, *74*, 085320.
(3) Early, K. T.; Sudeep, P. K.; Emrick, T.; Barnes, M. D. *Nano Lett.* **2010**, *10*, 1754.
(4) Huang, J.; Huang, Z.; Yang, Y.; Zhu, H.; Lian, T. *J. Am. Chem. Soc.* **2010**, *132*, 4858.
(5) Scholz, F.; Dworak, L.; Matylitsky, V. V.; Wachtveitl, J. *ChemPhysChem* **2011**, *12*, 2255.
(6) Morris-Cohen, A. J.; Frederick, M. T.; Cass, L. C.; Weiss, E. A. *J. Am. Chem. Soc.* **2011**, *133*, 10146.
(7) Morris-Cohen, A. J.; Peterson, M. D.; Frederick, M. T.; Kamm, J. M.; Weiss, E. A. *J. Phys. Chem. Lett.* **2012**, *3*, 2840.
(8) Yang, Y.; Rodríguez-Córdoba, W.; Lian, T. *Nano Lett.* **2012**, *12*, 4235.
(9) Sehgal, P.; Narula, A. k. *Opt. Mater.* **2015**, *48*, 44.
(10) Ellis, J. L.; Hickstein, D. D.; Schnitzenbaumer, K. J.; Wilker, M. B.; Palm, B. B.; Jimenez, J. L.; Dukovic, G.; Kapteyn, H. C.; Murnane, M. M.; Xiong, W. *J. Am. Chem. Soc.* **2015**, *137*, 3759.
(11) Jensen, S. C.; Homan, S. B.; Weiss, E. A. *J. Am. Chem. Soc.* **2016**, *138*, 1591.
(12) Boulesbaa, A.; Issac, A.; Stockwell, D.; Huang, Z.; Huang, J.; Guo, J.; Lian, T. *J. Am. Chem. Soc.* **2007**, *129*, 15132.
(13) Huang, J.; Huang, Z.; Jin, S.; Lian, T. *J. Phys. Chem. C* **2008**, *112*, 19734.
(14) Matylitsky, V. V.; Dworak, L.; Breus, V. V.; Basché, T.; Wachtveitl, J. *J. Am. Chem. Soc.* **2009**, *131*, 2424.
(15) Zhu, H.; Yang, Y.; Lian, T. *Acc. Chem. Res.* **2013**, *46*, 1270.
(16) Zhu, H.; Song, N.; Rodríguez-Córdoba, W.; Lian, T. *J. Am. Chem. Soc.* **2012**, *134*, 4250.
(17) Peterson, M. D.; Jensen, S. C.; Weinberg, D. J.; Weiss, E. A. *ACS Nano* **2014**, *8*, 2826.
(18) Bockman, T. M.; Kochi, J. K. *J. Org. Chem.* **1990**, *55*, 4127.
(19) Barnes, J. C.; Juríček, M.; Strutt, N. L.; Frasconi, M.; Sampath, S.; Giesener, M. A.; McGrier, P. L.; Bruns, C. J.; Stern, C. L.; Sarjeant, A. A.; Stoddart, J. F. *J. Am. Chem. Soc.* **2013**, *135*, 183.
(20) Dale, E. J.; Vermeulen, N. A.; Juríček, M.; Barnes, J. C.; Young, R. M.; Wasielewski, M. R.; Stoddart, J. F. *Acc. Chem. Res.* **2016**, *49*, 262.
(21) Ryan, S. T. J.; Young, R. M.; Henkelis, J. J.; Hafezi, N.; Vermeulen, N. A.; Hennig, A.; Dale, E. J.; Wu, Y.; Krzyaniak, M. D.; Fox, A.; Nau, W. M.; Wasielewski, M. R.; Stoddart, J. F.; Scherman, O. A. *J. Am. Chem. Soc.* **2015**, *137*, 15299.
(22) Young, R. M.; Dyar, S. M.; Barnes, J. C.; Juríček, M.; Stoddart, J. F.; Co, D. T.; Wasielewski, M. R. *J. Phys. Chem. A* **2013**, *117*, 12438.
(23) Dyar, S. M.; Barnes, J. C.; Juríček, M.; Stoddart, J. F.; Co, D. T.; Young, R. M.; Wasielewski, M. R. *Angew. Chem., Int. Ed.* **2014**, *53*, 5371.
(24) Fathalla, M.; Barnes, J. C.; Young, R. M.; Hartlieb, K. J.; Dyar, S. M.; Eaton, S. W.; Sarjeant, A. A.; Co, D. T.; Wasielewski, M. R.; Stoddart, J. F. *Chem. - Eur. J.* **2014**, *20*, 14690.
(25) Barnes, J. C.; Juríček, M.; Vermeulen, N. A.; Dale, E. J.; Stoddart, J. F. *J. Org. Chem.* **2013**, *78*, 11962.
(26) McArthur, E. A.; Morris-Cohen, A. J.; Knowles, K. E.; Weiss, E. A. *J. Phys. Chem. B* **2010**, *114*, 14514.
(27) Knowles, K. E.; Malicki, M.; Weiss, E. A. *J. Am. Chem. Soc.* **2012**, *134*, 12470.

DOI: 10.1021/jacs.5b13386
J. Am. Chem. Soc. 2016, 138, 6163−6170

(28) McConnell, H. M. *J. Chem. Phys.* **1956**, *24*, 632.
(29) McConnell, H. M. *J. Chem. Phys.* **1956**, *24*, 764.
(30) Klimov, V. I. *Nanocrystal Quantum Dots*, 2nd ed.; CRC Press: Boca Raton, FL, 2010.
(31) Grätzel, M.; Moser, J. *Proc. Natl. Acad. Sci. U. S. A.* **1983**, *80*, 3129.
(32) Moser, J.; Graetzel, M. *J. Am. Chem. Soc.* **1983**, *105*, 6547.
(33) Guyot-Sionnest, P.; Shim, M.; Matranga, C.; Hines, M. *Phys. Rev. B: Condens. Matter Mater. Phys.* **1999**, *60*, R2181.
(34) Klimov, V. I.; Mikhailovsky, A. A.; McBranch, D. W.; Leatherdale, C. A.; Bawendi, M. G. *Phys. Rev. B: Condens. Matter Mater. Phys.* **2000**, *61*, R13349.
(35) Guyot-Sionnest, P.; Wehrenberg, B.; Yu, D. *J. Chem. Phys.* **2005**, *123*, 074709.
(36) Klimov, V. I. *Annu. Rev. Phys. Chem.* **2007**, *58*, 635.
(37) Park, Y.-S.; Bae, W. K.; Pietryga, J. M.; Klimov, V. I. *ACS Nano* **2014**, *8*, 7288.
(38) Klimov, V. I.; McGuire, J. A.; Schaller, R. D.; Rupasov, V. I. *Phys. Rev. B: Condens. Matter Mater. Phys.* **2008**, *77*, 195324.
(39) Klimov, V. I. *Annu. Rev. Condens. Matter Phys.* **2014**, *5*, 285.
(40) ten Cate, S.; Sandeep, C. S. S.; Liu, Y.; Law, M.; Kinge, S.; Houtepen, A. J.; Schins, J. M.; Siebbeles, L. D. A. *Acc. Chem. Res.* **2015**, *48*, 174.

DOI: 10.1021/jacs.5b13386
J. Am. Chem. Soc. 2016, 138, 6163−6170